Title: A lack of GluN2A-containing NMDA receptors confers a vulnerability to redox dysregulation: Consequences on parvalbumin interneurons, and their perineuronal nets.

Authors: Cardis R, Cabungcal JH, Dwir D, Do KQ, Steullet P

Journal: Neurobiology of disease

Year: 2017

Issue: 109

Volume: Pt A

Pages: 64-75

DOI: 10.1016/j.nbd.2017.10.006

Title:

A lack of GluN2A-containing NMDA receptors confers a vulnerability to redox dysregulation: consequences on parvalbumin interneurons, and their perineuronal nets

Running title: A lack of GluN2A confers a vulnerability to redox dysregulation

Authors:

Romain Cardis, M.S., Jan-Harry Cabungcal, Ph.D., Daniella Dwir, Ph.D., Kim Q. Do, Ph.D., Pascal Steullet, Ph.D.

Affiliation:
Center of Psychiatric Neuroscience, Department of Psychiatry
Lausanne University Hospital (CHUV)
Site de Cery
1008 Prilly-Lausanne
Switzerland

Correspondence:
Pascal Steullet
Center of Psychiatric Neuroscience
Site de Cery
1008 Prilly-Lausanne
Switzerland
Phone: +41 (0)21 314 28 33
Fax: +41 (0)21 314 65 62
e-mail: pascal.steullet@chuv.ch

Keywords: oxidative stress, perineuronal net, parvalbumin interneuron, anterior cingulate cortex, glutahione, peroxiredoxin, sulfiredoxin, mouse, oscillations, microglia

Abstract

The GluN2A subunit of NMDA receptors (NMDARs) plays a critical role during postnatal brain development as its expression increases while Glun2B expression decreases. Mutations and polymorphisms in GRIN2A gene, coding for GluN2A, are linked to developmental brain disorders such as mental retardation, epilepsy, schizophrenia. Published data suggest that GluN2A is involved in maturation and phenotypic maintenance of parvalbumin interneurons (PVIs), and these interneurons suffer from a deficient glutamatergic neurotransmission via GluN2A-containing NMDARs in schizophrenia.

In the present study, we find that although PVIs and their associated perineuronal nets (PNNs) appear normal in anterior cingulate cortex of late adolescent / young adult GRIN2A KO mice, a lack of GluN2A delays PNN maturation. GRIN2A KO mice display a susceptibility to redox dysregulation as sub-threshold oxidative stress and subtle alterations in antioxidant systems are observed in their prefrontal cortex. Consequently, an oxidative insult applied during early postnatal development increases oxidative stress, decreases the number of parvalbumin-immunoreactive cells, and weakens the PNNs in KO but not WT mice. These effects are long-lasting, but preventable by the antioxidant, N-acetylcysteine. The persisting oxidative stress, deficit in PVIs and PNNs, and reduced local high-frequency neuronal synchrony in anterior cingulate of late adolescent / young adult KO mice, which have been challenged by an early-life oxidative insult, is accompanied with microglia activation.

Altogether, these indicate that a lack of GluN2A-containing NMDARs alters the fine control of redox status, leading to a delayed maturation of PNNs, and conferring vulnerability for long-term oxidative stress, microglial activation, and PVI network dysfunction.

1. Introduction

Parvalbumin-expressing interneurons (PVIs) are fast-spiking GABAergic neurons that form inhibitory synapses onto either cell body or axon initial segment of pyramidal neurons. Via feed-forward and feed-back inhibitions, these interneurons exert a precise temporal control on the information flowing through their target neurons. Interconnected PVIs constitute a neuronal network able to synchronize the excitatory state of large numbers of neurons (Bartos et al., 2007). Thus, PVIs coordinate the activity of neuronal assemblies in high-frequency synchrony (Cardin et al., 2009; Fuchs et al., 2007; Massi et al., 2012; Sohal et al., 2009), thereby modulating the processing of information required for sensory perception, working memory, attention, learning and memory, and social behavior (Billingslea et al., 2014; Hu et al., 2014).

Anomalies in PVIs and their associated networks are key pathological features of schizophrenia (SZ) (Beasley and Reynolds, 1997; Lewis et al., 2012). Moreover, the specialized extracellular matrix (perineuronal nets, PNNs), which envelops many PVIs, is also abnormal in this disease (Enwright et al., 2016; Mauney et al., 2013; Pantazopoulos et al., 2015). The immature developmental gene expression profile of PVIs in SZ (Gandal et al., 2012) suggests a defect in the proper phenotypic maturation of these interneurons, which are particularly sensitive to perturbations during brain development (Steullet et al., 2016). Some of the proposed mechanisms underlying PVI anomalies in SZ are aberrant wiring of PVIs within neuronal networks, impaired glutamatergic inputs onto these interneurons and deleterious effects of neuroinflammation and oxidative stress (Lewis et al., 2012; Steullet et al., 2016). Impaired NMDA receptor (NMDAR)-dependent signaling, which represents a major pathological pathway in SZ (Coyle et al., 2012; Poels et al., 2014; Steiner et al., 2013), affects PVIs (Behrens et al., 2007) and neuronal network activity (Carlen et al., 2012; Homayoun and Moghaddam, 2007; Kocsis et al., 2013; Korotkova et al., 2010). These interneurons are particularly sensitive to NMDAR antagonists during their development and maturation (Abekawa et al., 2007; Powell et

al., 2012; Wang et al., 2008). However, the contribution of the different subtypes of NMDARs to the effect of general NMDAR antagonists is not well established.

NMDARs, which are ionotropic glutamate receptors, are heterotetramers consisting of two obligatory GluN1 subunits and two variable subunits (GluN2A, GluN2B, GluN2C, GluN2D, GluN3A, or GluN3B). The subunit composition of NMDARs determines the kinetic of calcium entrance upon receptor activation and the nature of the activated intracellular signaling (Paoletti et al., 2013). Therefore, distinct subtypes of NMDARs convey different functions. The GluN2A subunit, whose expression increases during early postnatal life, is involved in cortical network refinement during development via its actions on structural and functional synaptic plasticity (Cho et al., 2009; Fagiolini et al., 2003). Cortical PVIs undergo an early postnatal and activity-dependent switch of the GluN2 subunit composition of NMDARs, with GluN2A becoming more numerous than GluN2B subunits (Matta et al., 2013; Zhang and Sun, 2011). The postnatal increase of GluN2A in PVIs coincides with the maturation of these interneurons and the PNN formation. Studies using antagonists targeting preferentially either GluN2A - or GluN2B-containing NMDARs suggest that GluN2A, not GluN2B, contribute to PVI maturation and phenotypic maintenance (Kinney et al., 2006; Zhang and Sun, 2011). A disrupted function of GluN2A-containing NMDARs, as suggested by genetic studies, might therefore result in aberrant maturation and function of PVIs in some patients. Indeed, a few mutations in GRIN2A, the gene encoding GluN2A, have been identified in SZ (Hardingham and Do, 2016; Tarabeux et al., 2011). The locus containing GRIN2A is also associated with schizophrenia in a large genome wide association study (Consortium, 2014). The high-risk polymorphisms of GT repeats on the GRIN2A promoter give rise to reduced transcription (Liu et al., 2015), and reduced GluN2A expression, have been reported in prefrontal cortex (Beneyto and Meador-Woodruff, 2008) and PVIs (Bitanihirwe et al., 2009).

Although pharmacological manipulations support a role of GluN2A in development and phenotyping maintenance of PVIs, a demonstration of such function via genetic deletion of

GRIN2A was missing. Moreover, how the GluN2A-mediated signaling disruption impact PVIs remain unclear. Redox dysregulation / oxidative stress, which is widely reported in schizophrenia (Do et al., 2009; Flatow et al., 2013; Kim et al., 2016; Yao and Keshavan, 2011), is a common endpoint of many genetic and environmental risk factors leading to defects in PVIs and their associated PNNs in the prefrontal cortex, namely the anterior cingulate cortex (ACC) (Steullet et al., 2017). In a recent perspective article, we briefly disclosed that PVI and PNN deficits are also accompanied with oxidative stress in GRIN2A KO mice. Here, we further explored the relationship between PVIs, PNNs and oxidative stress in the ACC of mice lacking GluN2A-containing NMDARs during postnatal development.

2. Methods

2.1. Animals.

GRIN2A KO mice (Sakimura et al., 1995) were provided by A. Lüthi (University of Lausanne). They were backcrossed with C57BL/6J mice through many generations and housed under a 12-hour light-dark cycle in groups of 3–5 individuals/cage. Experiments were performed on both sexes and approved by the Local Veterinary Office.

2.2. GBR12909 and N-acetylcysteine treatments

GBR12909 (GBR, 10 mg/kg i.p.) (BioTrend, Switzerland) was injected daily from postnatal days 10 to 20. The vehicle solution, a phosphate buffer saline solution (PBS), was used in control animals. N-acetylcysteine (NAC) (PharmaNAC, BioAdvantexPharma, Canada) was provided in drinking water (2.4 g/L) to the lactating mothers from postnatal days 7 to 20 (das Neves Duarte et al., 2012).

2.3. Perfusion and tissue preparation

For immunohistochemistry, mice were anesthetized and perfused with 4% paraformaldehyde. Coronal frozen sections (50-µm thick) of fixed brains were prepared and stored in ethylene glycol at -20 °C until use. For mRNA quantification, Western blots and GSH measurements, brains were quickly dissected out and sliced (2-mm thick) using a brain matrix. Slices were immediately stored at -80°C until use. Tissue from the medial prefrontal cortex was extracted from frozen brain slices using a tissue punch.

2.4. Immunohistochemistry

Triple immunolabeling for oxidative stress, parvalbumin (PV), and perineuronal nets (PNNs) was performed as followed. An antibody against 8-oxo-2'-deoxyguanosine (8-oxo-dG), a product of DNA oxidation, was used as oxidative marker, while the PNNs were labeled with the lectin Wisteria Floribunda Agglutinin (WFA), which binds the N-acetylgalactosamines in chondroitin sulfate proteoglycans (Berretta et al., 2015; Wang and Fawcett, 2012). Brain sections containing the anterior cingulate cortex (ACC) were first incubated with PBS + Triton 0.3% + sodium azide (1g/L) containing 2-3% normal horse serum, then placed for 48 hours in a solution with a mouse monoclonal anti-8-oxo-dG (1:400; AMS Biotechnology, Switzerland) and a rabbit polyclonal anti-parvalbumin (PV) (1:2500; Swant Inc, Switzerland) primary antibody together with the biotin-conjugated WFA (1:2000; Sigma, Switzerland). Sections were then washed, incubated with fluorescent secondary antibody conjugates: goat anti-mouse Alexa 488 (1:300; Life Technologies, USA), goat anti-rabbit CY3 (1:300; Chemicon International, USA) and streptavidin 405 conjugate (1:300; Millipore Corporation, USA). For dual immunolabeling of Iba1 and CD68 to label microglia, normal donkey serum (2%) was used as blocking agent. Primary antibodies were a goat polyclonal anti-Iba1 (1:1000; Abcam, UK) and a rat monoclonal anti-CD68 (1:1500; Abcam) antibody. Secondary antibody conjugates were a chicken anti-goat Alexa 594 (1:300; Life Technologies, USA) and a chicken anti-rat Alexa 488 (1:300; Life Technologies, USA).

Sections were visualized and processed with a Zeiss confocal microscope equipped with x10, x40 and x63 Plan-NEOFLUAR objectives. All peripherals were controlled with LSM 710 Quasar software (Carl Zeiss AG, Switzerland). With the triple immunolabeling of 8-oxo-dG, PV, and WFA, Z-stacks of 12 images (with a 2.13 µm interval) were scanned (1024 x 1024 pixels). Images were filtered with a Gaussian filter to remove background noise and sharpen cell profile contour. Only the inner 8 images of Z-stacks were used for the analyses. The stack images were merged in a tif file with Imaris, and further analyzed with Image J. Analyses were performed in a delineated region of interest (ROI) comprising the ACC (cg1) by an observer unaware of the experimental groups. For PV-IR, the number of PV-IR cell bodies was counted and the mean intensity of labeling (arbitrary unit) was measured separately within PV-IR cell bodies and PV-IR processes. PV-IR processes included all PV-labeled voxels that were not part of the identifed PV-IR cell bodies. The mean intensity (arbitrary unit) was used as a measure for 8-oxo-dG-IR and WFA labeling. Because the image acquisition, the defined ROI, and the image analysis were slightly different to those used in Steullet et al. (2017), the intensity of 8-oxo-dG (arbitrary unit) and the numbers of PV-IR cells / ROI in the present study were not identical to those reported in the above article. However irrespective of the analytical method used, the differences between experimental groups were similar. The number of PV-IR neurons surrounded by WFA-labeled PNNs was also counted in IMARIS software (Bitplane AG, Switzerland) as described previously (Cabungcal et al., 2013a). Data are based on 4 non-contiguous sections per mouse. For dual Iba1 and CD68 immunolabeling, Z-stacks of 20 images (with a 1.2 µm interval) were scanned. The numbers of immunoreactive cells in the ACC ROI, using only the inner 18 images of Z-stacks, were counted using the spot tool of IMARIS. Data are based on two non-contiguous sections per mouse.

2.5. mRNA quantification

RNAs were extracted from the medial prefrontal cortex using RNeasy Mini Kit (Qiagen, Germany) as described in the manufacturer's protocol. cDNA were synthesized using 300 ng

RNA in a reaction mixture containing RT-buffer 10x, 5.5 mM $MgCl_2$, 2 mM dNTP, 0.4 U/µl RNase Inhibitor, 2.5 µM Random Hexamers, and 1.25 U/µl RTase (Thermo Fisher Scientific, Waltham, USA). Taqman real time PCR was performed in a final volume of 20 µl containing 10 ng cDNA, 1 µl of selected probes mixed with 10 µl of TaqMan Universal PCR Master Mix (Thermo Fisher Scientific). Probes used were: GPX1 (Mm00656767_g1), GCLM (Mm00514996_m1), GCLC (Mm00802655_m1), TXNIP (Mm01265659_g1), SRXN1 (Mm00769566_m1), PPARGC1A (Mm01208835_m1), RPL27 (Rn00821099_g1), and β-Tubulin (TBB5) (Mm00495806_g1). Quantitative PCR was performed on Thermofisher 7500 Real-Time PCR System and the 7500 System SDS Software as established by the provider. Samples were run in duplicate. Values were normalized to the internal controls TBB5 and RPL27, and to a mixture of prefrontal samples. Data were analyzed using the ΔΔCt method.

2.6. Western Blots

Tissue from the medial prefrontal cortex were lysed in RIPA buffer (50 mM Tris-HCl, 150 mM NaCl, 1% SDS, 1mM dithiothreitol, 1 mM EDTA, 0.1% Triton, 0.6 mM phenylmethanesulfonyl fluoride, 30 mM NaF, 30 mM β-glycerophosphate, 0.2 mM orthovanadate and protease inhibitor cocktail (Roche)), sonicated and centrifuged for 15 min at 10000 g. Tissue lysates were boiled at 95°C for 10 min in loading buffer (0.5 M Tris pH 6.8, Glycerol 30%, SDS 10%, beta-mercaptoethanol 5%, bromophenol blue 0.012%). Proteins were separated by SDS-PAGE on 12.5% nitrocellulose membranes, and transferred on PVDF membranes. After blocking in Tris-buffered saline (TBS) containing 2.5% milk, membranes were incubated overnight at 4°C with primary antibodies diluted in TBS with 01% Tween 20 and 3% BSA, followed by 1-h incubation with fluorescent secondary antibodies and a subsequent wash with TBS. Signals were visualized and analyzed with an Odyssey Clx imaging system (LI-COR Biosciences, Lincoln, USA) using β-actin for normalization. 2-cys peroxiredoxins (Prxs) were labeled irrespective of their redox state using a mouse anti-2-Cys Prxs (1:1000, Abcam), while the hyperoxidized Prxs (Prx-$SO_{2/3}$H) were visualized with a rabbit anti-Prx-$SO_{2/3}$H (1:2000,

Abcam). Normalization was performed using a mouse anti-β-actin (1:20000, Abcam). Secondary antibodies were IRDye 800CW Goat anti-Mouse IgG (H + L) (1:10000, LI-COR Biosciences), IRDye® 680RD Goat anti-Rabbit IgG (H + L) (1:10000, LI-COR Biosciences).

2.7. GSH and oxidized GSH (GSSG) quantification

GSH and GSSG contents in medial prefrontal cortex were measured using the colorimetric Tietze method. Briefly, tissue was sonicated in ice-cold PBS (150 mM NaCl, 3 mM KCl, 1.5 mM KH_2PO_4, 7.9 mM Na_2HPO_4, , 2.5 mM EDTA, pH=7.4). An aliquot was immediately reserved for protein quantification with the Advanced Protein Assay (Cytoskeleton, Denver, CO, USA). In the remaining lysate, proteins were precipitated by adding 10% sulfosalicylic acid (for a final 0.5% solution). The lysate was then centrifuged for 10 min at 10000 rpm at 4°C and triethanolamine was added to the collected supernatant to adjust the pH to ~7.4. For the measurement of total GSH, an aliquot of supernatant was mixed with a freshly-made reaction solution containing at final concentration 0.5 U/ml GSH reductase from baker's yeast (Sigma, St-Louis, MO, USA), 0.15 mM DTNB, 0.15 mM NADPH, and 1 mM EDTA. The rate of increase in absorbance at 405 nm, which measures the reduction of DTNB by GSH, is proportional to the total GSH. GSSG measurement was performed as for the total GSH. However, 2-vinylpyridine was first added to an aliquot of supernatant (final solution 1.8%) to derivatize GSH (1-h incubation) so only GSSG remained available for the reaction. For each sample, total GSH and GSSG were measured in duplicates. Concentrations of total GSH or GSSG in supernatants were determined by comparison with dilution series of GSH and GSSG solutions, respectively. Total GSH and GSSG contents in tissue were expressed in nmol/mg protein.

2.8. Electrophysiology

Mice were anesthetized with a mixture of ketamine/xylazine, and intracardiacally perfused with oxygenated sucrose-containing artificial cerebrospinal fluid (ACF) (in mM: 252 sucrose, 3 KCl, 2 $MgSO_4$, 1.2 $CaCl_2$, 1.2 NaH_2PO_4, 24 $NaHCO_3$, 10 glucose; pH 7.4) for ~10

min prior to decapitation. Paracoronal slices (400-µm thick, Bregma ~1.4-0.6) containing the ACC were prepared with a vibroslicer in cold oxygenated sucrose-containing ACF, transferred into a “Haas” type interface chamber and superfused with oxygenated normal ACF (in mM: 126 NaCl, 3 KCl, 1 $MgCl_2$, 1.2 $CaCl_2$, 1.2 NaH_2PO_4, 24 $NaHCO_3$, 10 glucose; pH 7.4). ACF temperature was slowly raised from room temperature to ~32°C. Electrophysiological recordings were performed at least 90 min after slicing. An ACF-filled glass electrode (~5 MΩ) was placed in the superficial part of layer V of the dorsal ACC (Cg1). Signals were band pass-filtered at 1-1000 Hz and digitized at 2 kHz. Oscillatory neuronal activity was generated with a mixture of kainate (0.8 µM), carbachol, (50 µM), and quinpirole (1 µM) in 5 mM KCl-containing ACF (Steullet et al., 2014). Using the Welch method (IgorPro6 WaveMetrics, Portland, OR, USA), analysis of the power spectrum analyses was performed on a 60-sec recording taken after 25-35 min incubation with the mixture of receptor agonists. The power spectrum was normalized so the power density between 100 and 1000 Hz was identical across recordings. The power density of fast oscillatory activity was calculated within the β band frequency (12-28 Hz). For each mouse, recordings were done bilaterally within 2 consecutive slices. Recordings that failed to display oscillatory activity with a peak frequency higher than 15 Hz were excluded from the final analysis.

2.9. Statistics

Statistics were performed with the SPPS software (IBM). Normality was tested by the Shapiro-Wilk test. When the variances were homogenous based on Levene’s test, data were analysed using univariate or multivariate analyses (general linear model), or Student t-test. Post hoc multiple comparisons were then performed using the Tukey HSD test. When the homogeneity of variances was not met, the Games-Howell test for multiple comparisons and the Welch’s t-test were used. Quantification of mRNA expression was analyzed using a multivariate analysis (general linear model) with genotype and treatment as factors.

3. Results

3.1. Delayed maturation of PVIs and PNNs in GRIN2A KO mice

We first examined by immunohistochemistry parvalbumin-immunoreactive (PV-IR) neurons and PNNs in the ACC of GRIN2A KO and WT mice, at early postnatal age (PD20) and late adolescence / early adulthood (PD60). In WT mice, GluN2A is well expressed at PD20 (Matta et al., 2013; Zhang and Sun, 2011) when PVIs / PNNs undergo maturation. While the number of PV-IR cells did not differ between genotypes at both ages (Fig. 1a, 2), the intensity of PV-IR in processes was significantly lower in young GRIN2A KO mice (Fig. 1b, 2). Similar effect was observed regarding PV-IR intensity (a.u.) in soma: PD20 KO mice displayed significantly weaker PV-IR labeling (43 ± 2,mean ± sem) as compared to PD60 KO (56 ± 1, p=0.001) and to PD60 WT mice (55 ± 3, p=0.005). Likewise, PNN intensity was weaker in PD20, but not PD60 KO, as compared to age-matched WT mice (Fig. 1c, 2). The proportion of PV-IR cells wrapped with WFA-labeled PNNs was also lower in KO compared to WT mice at both ages (PD20: 57.2 ± 0.6 % in WT and 51.4 ± 1.1 % in KO (mean ± sem), p=0.004; PD60: 53.0 ± 1.1 % in WT and 48.7 ± 0.4 % in KO, p=0.004, two-tailed Student t-test, Bonferroni corrected for multiple comparisons). These data indicate that absence of GluN2A delays maturation of PV-IR and PNNs. We also assessed oxidative stress in the ACC using an antibody against 8-oxo-dG. At both PD20 and PD60, we found no significant difference of 8-oxo-dG-IR between genotypes (Fig. 1d, 2), although 8-oxo-dG-IR intensity was slightly more elevated in KO mice at both ages, as compared with age-matched WT mice. .

3.2. PVIs and PNNs are vulnerable to an early postnatal oxidative insult in GRIN2A KO mice

The fact that the ACC of GRIN2A KO mice showed a delayed maturation of PNNs known to protect PVIs against oxidative stress (Cabungcal et al., 2013b), suggested that an

early-life oxidative insult might be detrimental to PVIs. This hypothesis was tested by applying an oxidative insult consisting of a daily treatment (from PD10 to 20) with the dopamine uptake inhibitor, GBR12909 (GBR). GBR elevates extracellular dopamine levels causing a subsequent generation of reactive oxygen species (ROS) and reactive compounds resulting from dopamine catabolism and auto-oxidation (Hastings et al., 1996; Hirrlinger et al., 2002). Immediately following the 10-days treatment, GBR-treated KO mice displayed significantly higher 8-oxo-dG-IR in the ACC as compared to both WT groups (Fig. 3d, 4). The number of PV-IR cells and the intensity of PV-IR in processes were also significantly lower in GBR-treated KO mice, as compared to PBS- and GBR-treated WT mice (Fig. 3a,b, 4). PV-IR intensity in soma was also significantly lower in GBR-treated KO (46 ± 2) as compared to PBS-treated WT mice (56 ± 2, p=0.023). Likewise, the intensity of WFA-labeled PNNs was weaker in GBR-treated KO mice than in both WT groups (Fig. 3c, 4). Thus, a postnatal oxidative insult in KO mice increases oxidative stress, which is accompanied with reduction in number of PV-IR cells, further weakening of PV-labeling and WFA-labeled PNNs. The antioxidant, N-acetylcysteine (NAC), provided from PD7 to PD20, was sufficient to prevent all GBR effects in KO mice (Fig. 3e-h, 4). Noteworthy, NAC restored PNNs to levels observed in naïve (Fig. 1c), or PBS-treated WT mice (Fig. 3c). Taken together, this shows that absence of GluN2A favors a susceptibility to oxidative stress-induced PVI / PNN defects.

3.3. Weakened antioxidant defenses in GRIN2A KO mice

As oxidative stress becomes prominent in the ACC of GRIN2A KO mice following a GBR treatment, we then explored the possible cause of such susceptibility to redox dysregulation. One hypothesis is that absence of GluN2A slightly compromises antioxidant systems. Synaptic NMDARs are indeed coupled with transcriptional control of several antioxidant systems (Baxter et al., 2015; Papadia et al., 2008). Therefore, we quantified the expression of genes implicated in the glutathione system (i.e., GCLC, GCLM, GPX1), thioredoxin system (i.e., TXNIP) and

peroxiredoxin (Prx) system (i.e., SRXN1) (Fig. 5), as well as in mitochondria and antioxidant support (i.e., PPARGC1a) in medial prefrontal cortex of PD20 WT and KO mice treated either with GBR or PBS. The expression of these genes are affected by pharmacologically-induced NMDAR hypofunction (Baxter et al., 2015; Jiang et al., 2013; Papadia et al., 2008). A multivariate analysis revealed a genotype ($p=0.021$), but no treatment effect and no interaction (Fig. 6a). In particular, there was a genotype effect on the expression of GCLM ($p=0.003$) and SRXN1 ($p=0.007$), which were both lower in KO compared to WT mice (Fig. 6a). GCLM codes for the modulatory subunit of the glutamate-cysteine ligase, the key synthesizing enzyme of glutathione (GSH), while SRXN1 codes for sulfiredoxin 1 whose function is to reduce hyperoxidized Prxs (Prx-$SO_{2/3}$H). Moreover, the lowest expression of 4 out of the 6 investigated genes was found in GBR-treated KO mice (Fig. 6a). Thus, the absence of GluN2A decreases the transcription of some genes associated with the antioxidant defenses. Because of the reduced transcription of GCLM and SRXN1 in KO mice, we then examined whether levels of GSH, Prxs, and their respective redox state were altered in KO mice. Despite a reduced GCLM gene expression in KO mice, the total GSH content (sum of reduced and oxidized forms) was not different in both genotypes and not affected by the treatment (Fig. 6b). However, the level of oxidized GSH (GSSG) was significantly higher in GBR-treated KO mice as compared to PBS-treated WT mice (Fig. 6c). Regarding the Prxs, we found that GBR treatment increased the amount of Prxs (~21 kDa band corresponding to Prx 1 and Prx 2) in WT but not in KO mice (Fig. 6d,f). The ratio between hyperoxidized Prxs (Prx-$SO_{2/3}$H) and total Prxs (2-Cys Prx) was not significantly different between groups, although hyperoxidation tended to be higher in GBR-treated KO mice (Fig. 6e,f). Thus in KO mice, the impaired upregulation of Prxs in response to GBR may limit the capacity of the Prx system to neutralize ROS. This may account for the more oxidized redox states of GSH and Prxs, as well as higher 8-oxo-dG-IR in GBR-treated KO mice. These results indicate that a lack of GluN2A is accompanied with subtle alterations in gene or

protein expression of key elements of the GSH and Prx systems, which may contribute to the greater vulnerability of GRIN2A KO mice to oxidative insults as compared to WT mice.

3.4. An early postnatal oxidative insult has long-term effects on PVI and PNN integrity in GRIN2A KO mice

As early environmental stressors can cause long-term brain alterations in individuals with genetic susceptibility, we investigated the long-term effects of an early-life oxidative insult on the integrity of PVIs and PNNs in the ACC of PD60 GRIN2A KO mice. Previously, we have shown that a postnatal GBR treatment had no long-term effects on oxidative stress and PVI / PNN integrity in ACC of WT mice (Cabungcal et al., 2013a). Therefore, we only compared GBR-treated KO mice with non-treated KO and WT mice. We observed that 8-oxo-dG-IR was significantly higher in GBR-treated KO than in non-treated KO and WT mice (Fig. 7d, 8). The number of PV-IR cells, the intensity of PV-IR in processes and WFA-labeling were lower in GBR-treated KO mice compared to the other groups (Fig. 7a-c, 8). PV-IR intensity in soma was also significantly lower in GBR-treated KO compared to PBS-treated KO mice (48 ± 2 vs. 56 ± 1, p=0.011). The proportion of PV-IR cells enveloped with WFA-labeled PNNs was also lower in GBR-treated KO (40.9 ± 2.4 %, mean ± sem) compared to non-treated WT (53.0 ± 1.1 %) and KO mice (48.7 ± 0.4 %) (p=0.002 and p=0.02, respectively, two-tailed Student t-test, Bonferroni corrected for multiple comparisons). These data demonstrate that an early-life oxidative insult causes persistent oxidative stress together with long-lasting impact on PVI and PNN integrity in the ACC of GRIN2A KO mice.

3.5. An early postnatal oxidative insult causes long-term microglia activation in GRIN2A KO mice

Since an early-life GBR treatment caused a long-term increase in oxidative stress in the ACC of KO mice, we explored whether this was accompanied with a persisting activation of microglia. Assessment of microglia was performed by immunohistochemistry using an antibody against Iba1, a microglia/macrophage-specific marker, and an antibody against CD68, a glycoprotein highly expressed in activated microglia. We found a significant difference in the number of CD68-IR cells, but not Iba1-IR cells, between PD60 non-treated WT and KO mice (Fig. 7e,f, 9). But most notably, the numbers of Iba1-IR and CD68-IR cells were higher in GBR-treated KO mice as compared to non-treated WT and KO mice. Such effect of GBR on microglia was not observed in WT mice (Dwir et al. Society of Neuroscience abstract 2016). Moreover, Iba1-IR cells in GBR-treated KO mice displayed amoeboid shapes. These indicate that GRIN2A KO mice show a vulnerability for microglia activation and that an early-life oxidative insult promotes long-term phagocytic-like state of microglia in these mice.

3.6. An early postnatal oxidative insult has a modest long-term effect on local fast oscillatory neuronal activity in GRIN2A KO mice

We examined whether local fast oscillatory neuronal activity in the ACC of PD60 GRIN2A KO mice was also affected by an early-life GBR treatment. High-frequency oscillations (in β range: 12-28Hz) were induced pharmacologically in ACC slices with the superfusion of carbachol, kainate and quinpirole. This fast oscillatory activity requires $GABA_A$ and AMPA receptors, as well as gap junctions (Steullet et al., 2014), and is impaired when there is a reduced number of PV-IR cells in a mouse model of redox dysregulation (Cabungcal et al., 2013b). First, we checked whether GBR had an effect on high-frequency oscillations in WT mice. We found no difference in oscillation power and peak frequency between PBS- and GBR-treated WT mice (Fig. 10a,c,e). By contrast, GBR significantly decreased the oscillation power in KO mice ($p=0.009$, one-tailed t-test; Fig. 10b,d), but had no effect on the peak frequency (Fig.

10f). Together, this indicates that an early-life oxidative insult impacts modestly local high-frequency oscillations in the ACC of late adolescent / young adult GRIN2A KO mice.

4. Discussion

This study reveals that a lack of GluN2A leads to sub-threshold oxidative stress and delays maturation of PNNs and PVIs in the ACC. These effects appear to be caused by a dysregulated modulation of antioxidant systems. Consequently, an early-life oxidative insult results in persistent oxidative stress, microglia activation, decrease in PV-IR and WFA-labeled PNN integrity.

Our finding that GluN2A favors PNN and PVI maturation is consistent with the notion that NMDAR subunit plays an important role in cortical network refinement during postnatal development. GluN2A deletion impairs the development of orientation preference through sensory experience and weakens cortical plasticity to monocular deprivation in visual cortex (Fagiolini et al., 2003). This plasticity can be restored by diazepam indicating an excitation / inhibition imbalance in young GRIN2A KO mice. While studies using a GluN2A-containing NMDAR antagonist suggest that GluN2A is implicated in both PVI maturation and phenotypic maintenance (Kinney et al., 2006; Zhang and Sun, 2011), we demonstrate in this study that this receptor subtype plays an essential role in PVI maturation, but not phenotypic maintenance. Thus, a lack of GluN2A delays maturation of PNNs and PV-IR without impacting PV-IR and PNNs at late adolescence / early adulthood. PNN expression depends on neuronal activity (McRae et al., 2007) and requires calcium signaling (Dityatev et al., 2007). Here, we show that the antioxidant NAC prevents the delayed PNN formation in GRIN2A KO mice. This strongly suggests that the slowing down of PNN maturation in absence of GluN2A is mostly driven by a redox dysregulation as evidenced by a sub-threshold level of oxidative stress, which is known to delay WFA-labeled PNN formation (Cabungcal et al., 2013b). However, we cannot fully exclude

that the boosting effect of NAC on PNN maturation in KO mice occurs via an upregulation of the glial glutamate transporter GLT-1 and the cystine-glutamate exchanger xCT (McClure et al., 2014), leading to changes in extracellular glutamate levels and in activation of synaptic and extrasynaptic glutamate receptors also involved in PNN maturation. Our results suggest that the redox dysregulation in GRIN2A KO mice is caused by altered modulation of several antioxidant systems, including the GSH and Prx systems. Activation of synaptic NMDARs indeed regulates the transcription of genes associated with the GSH, Prx, and thioredoxin systems to support antioxidant defense and redox control in an activity-dependent manner (Baxter et al., 2015; Papadia et al., 2008). The expression of genes associated with several antioxidant systems and mitochondrial function is impaired upon conditional deletion of the NR1 subunit in forebrain interneurons (Jiang et al., 2013). NMDARs can modulate antioxidant systems via multiple transcription factors (e.g. CREB, FOXO, ATF4) (Papadia et al., 2008). It is therefore possible that not one, but several pathways are slightly dysregulated by a lack of GluN2A. Indeed, further investigations will be required to identify the pathway(s) responsible for the subtle dysregulation of the antioxidant defense in GRIN2A KO mice. Additionally, a lack of GluN2A might reinforce the impact of GluN2B-mediated signaling cascades in neurons, one of them leading to NADPH oxidase-mediated superoxide production (Costa et al., 2012). For example, a specific GluN2A antagonist increased superoxide production in prefrontal cortex of young mice (Powell et al., 2012). Our data suggest that GluN2A-containing NMDARs sense network activity to maintain adequate redox control, which is particularly critical during postnatal development. Collectively, the present study proposes a novel mechanism by which GluN2A-containing NMDARs not only determines the direction of synaptic plasticity (Cho et al., 2009) but also mildly regulates redox-sensitive molecular mechanisms involved in cortical development and refinement. This includes regulation of the building up and maturation of PNNs. Environmental enrichment (EE) is also known to delay PNN development and modulate PNN integrity and composition. Depending on brain regions, EE weakens or enhances PNNs (Foscarin et al., 2011; Slaker et al., 2016).

However, the dynamic regulation of synthesis and removal of extracellular matrix components by EE likely involve mechanisms independent of oxidative stress.

The perturbed redox regulation and PNN deficit in ACC of PD20 GRIN2A KO mice also confer an increased susceptibility to an early-life oxidative insult. Previously, we have shown that a treatment with GBR leads to an excess of oxidative stress in ACC of young mice with a GSH deficit, but not in WT mice (Cabungcal et al., 2013a). Likewise, a GBR treatment increases oxidative stress and decreases PV-IR and PNN integrity in ACC of PD20 GRIN2A KO. The GBR effects are prevented by NAC, proving the pivotal role of redox dysregulation. This is consistent with the notion that redox dysregulation / oxidative stress constitutes a convergent pathological pathway causing PNN / PVI anomalies in many animal models relevant to SZ (Steullet et al., 2017). In GRIN2A KO mice, the impaired upregulation of Prxs in response to GBR may compromise the ability to adequately neutralize an excess of ROS production, leading to oxidative stress, PV-IR decrease and PNN deficit. Remarkably, the increased oxidative stress induced by an early-life GBR treatment persists until late adolescence / young adulthood together with the reduction of PV-IR, weakening of WFA-labeled PNNs, and activation of microglia in a phagocytic-like state. The reason for the persistence of oxidative stress and microglia activation following an early-life oxidative insult in GRIN2A KO mice might be directly linked to their sub-optimal antioxidant and redox regulation capacities. While an impaired redox regulation favors oxidative stress and microglia activation during an oxidative insult (i.e., GBR treatment), it may likewise prevent these glial cells to return into their inactivated state. Indeed, the phenotype of microglia is tightly regulated by the thiol redox status (Rojo et al., 2014), whereby an appropriate reduced redox state is necessary for microglia inactivation. In a feed-forward process, the failure of microglia to switch back into a “resting” phenotype after being activated by an early insult could in turn maintain long-lasting oxidative stress leading to persistent PVI and PNN deficits.

In psychiatric diseases such as SZ, abnormal glutamatergic transmission, oxidative stress and microglia activation are commonly reported. The present study demonstrates that NMDAR hypofunction can be an upstream event of oxidative stress and neuroinflammation. This does not rule out, however, other possible scenarios whereby redox dysregulation or neuroinflammation could be primary cause for the disruption of the homeostasis between these tightly and reciprocally interconnected systems. In this context, the GluN2A subunit may play a pivotal role. Altered GluN2A expression is reported following social isolation, which also induces oxidative stress and microglia activation (Schiavone et al., 2012; Turnock-Jones et al., 2009): this might represent adaptive and/or compensatory mechanisms to stressors. Interestingly, GluN2A-containing NMDARs are themselves redox-sensitive and their function diminishes under oxidative conditions (Choi et al., 2001; Kohr et al., 1994). A priori, this appears counterintuitive as GluN2A contributes to the regulation of antioxidant capacity and redox balance. One hypothesis is that a strong GluN2A-mediated signaling could be deleterious in some conditions. For instance, an overexpression of GluN2A in prefrontal cortex during adolescence is responsible for the anxious behavior and the decreased number of PV-IR cells caused by a maternal separation in rats (Ganguly et al., 2015).

5. Conclusions

To conclude, a lack of GluN2A-dependent signaling confers a vulnerability to early-life stressors that affect PVIs and extracellular matrix via an inappropriate regulation of redox and immune systems. This could be relevant to SZ and but also other neurodevelopmental disorders associated with GRIN2A mutations such as epilepsy-aphasia. In the latter syndrome, same GRIN2A gene mutation can cause mild to severe symptoms, suggesting that other genetic and environment factors may play a role in the severity of the pathology (Burnashev and

Szepetowski, 2015; Hardingham and Do, 2016). Thus, antioxidant could be potentially beneficial to patients with a defect in GluN2A-containing NMDARs.

Funding Information

The authors would like to acknowledge the support of the Swiss National Science Foundation (# 310030_135736/1 to KQD and PS), National Center of Competence in Research (NCCR) "SYNAPSY - The Synaptic Bases of Mental Diseases" from the Swiss National Science Foundation (n° 51NF40-158776), Pro Scientia et Arte, Juchum Foundation, Damm-Etienne Foundation and Alamaya Foundation.

Conflict of interest

The authors declare no conflict of interest.

Acknowledgments: We would like to thank Adeline Cottier and Hélène Moser for their helpful technical support, and Anita Lüthi for kindly providing us the GluN2A KO mice. We thank our financial supports: Swiss National Science Foundation # 310030_135736/1 to KQD and PS), National Center of Competence in Research (NCCR) "SYNAPSY - The Synaptic Bases of Mental Diseases" from the Swiss National Science Foundation (n° 51NF40-158776), Pro Scientia et Arte, Juchum Foundation, Damm-Etienne Foundation and Alamaya Foundation.

Figure legends

Fig. 1. Delayed maturation of parvalbumin interneuron processes and perineuronal nets (PNNs), and sub-threshold oxidative stress in the anterior cingulate cortex (ACC) of GRIN2A KO mice. A Number of parvalbumin-immunoreactive (PV-IR) cells in ROI delineating the ACC. **B** Intensity (a.u.) of PV-IR within processes. **C** Intensity (a.u.) of labeling of WFA-PNNs. **D** Intensity (a.u.) of 8-oxo-dG-IR. Box plots depict medians and quartiles; bars show values in the 1.5 box length range. WT at PD20 (2 males, 2 females); WT at PD60 (2, 3); KO at PD20 (3, 3); KO at PD60 (6, 2). * $p<0.05$, ** $p<0.01$, *** $p<=0.001$ (multiple comparisons using either Tukey HSD test or Games-Howell test).

Fig. 2. A Representative images of parvalbumin, WFA, and 8-oxo-dG labeling in the ACC of PD20 WT and GRIN2A KO mice. Scale: 50 µm. **B** Higher magnification images showing PV-IR processing in superficial and deep layers of both WT and KO mice. Scale: 20 µm. **C** Higher magnification image illustrating the WFA staining associated with PV-IR cells. Scale: 20 µm. Note that in both B and C, the PV labeling was enhanced for display purpose only in order to better show PV-IR processes. Therefore, PV labeling in soma appears saturated in these images. **D** Schema showing the region of interest (ROI) in the ACC (cg1) in which quantification of PV-IR, 8-oxo-dG-IR and WFA staining was performed. CC: corpus callosum.

Fig. 3. Early-life treatment with the dopamine uptake inhibitor, GBR12909 (GBR), increases oxidative stress, and affects parvalbumin interneurons and perineuronal nets (PNNs) in the ACC of PD20 GRIN2A KO mice. A Number of parvalbumin-immunoreactive (PV-IR) cells. **B** Intensity (a.u.) of PV-IR within processes. **C** Intensity (a.u.) of labeling of WFA-PNNs. **D** Intensity (a.u.) of 8-oxo-dG-IR. WT PBS (5 males, 2 females); WT GBR (4, 3); KO PBS (3, 3); KO GBR (3, 4). **E-H** Treatment of KO mice with N-acetylcysteine (NAC) prevents

GBR-induced oxidative stress (**H**), reduction in number of PV-IR cells (**E**) and PV-IR intensity in processes (**F**), and re-establishes normal levels of WFA-labeled PNNs (**G**). For **A-D**: * p<=0.05, ** p<=0.01, *** p<=0.001 (multiple comparisons using the Tukey HSD test). For **E-H**: ***: p<0.0005 (two-tailed Student or Welch's t-test). KO GBR (3 males, 2 females), KO GBR+NAC (4, 4). Box plots depict medians and quartiles; bars show values in the 1.5 box length range.

Fig. 4. Effect of early-life treatment with the dopamine uptake inhibitor, GBR12909 (GBR) on oxidative stress, parvalbumin interneurons, and perineuronal nets (PNNs) in the ACC of PD20 GRIN2A KO mice. Representative images of parvalbumin immunoreactivity, WFA-labeled PNNs, and 8-oxo-dG labeling in the ACC of PBS- treated and GBR-treated WT mice, PBS-treated and GBR-treated KO mice, and GBR-treated KO mice treated with N-acetylcysteine (NAC). Scale: 50 μm.

Fig. 5. Simplified scheme of the glutathione (GSH), thioredoxin (Trx), and peroxiredoxin (Prx) systems. Enzyme names are given in italic. GPx, glutathione peroxidase; GR, glutathione reductase; TrxR, thioredoxin reductase; Cys, cysteine; Glu, glutamate; Glu-Cys, glutamylcysteine; GSSG, oxidized GSH; Txnip, thioredoxin-interacting protein. Txnip interacts with reduced Trx to block the reduction by Trx of its substracts (e.g. oxidized 2-Cys Prxs). Here, Prx represent only the 2-cys Prxs. For simplification, only one of the sulfur group from the two cys residues in the Prx is presented in its different redox states (reduced: -SH, sulfenic: -SOH, sulfinic: $-SO_2H$, disulfide: S-S). R can be a Prx or other molecules interacting with oxidized Prx to form disulfide bridges.

Fig. 6. Regulation of antioxidant systems is altered in GRIN2A mice. A Expression of genes associated with antioxidant systems and mitochondrial support in the medial prefrontal cortex of

PBS- and GBR-treated WT and KO mice (at PD20). Values are expressed relative to the average expression in WT PBS mice after normalization using TBB5 and RPL27 as internal controls. Multivariate analysis shows a genotype effect on GCLM ($F[1,35]=9.918$; $p=0.003$) and SRXN1 ($F[1,35]=8.366$; $p=0.007$) expression. WT PBS (5 males, 5 females); WT GBR (6, 4); KO PBS (5, 5); KO GBR (4, 5). * indicates significant difference with WT. **B-E** Content of GSH and 2-Cys peroxiredoxins (Prxs), and their redox state in the medial prefrontal cortex of PBS- and GBR-treated WT and KO mice (at PD20). **B** Content in total GSH and **C** oxidized GSH (GSSG). WT PBS (3 males, 3 females); WT GBR (3, 3); KO PBS (3, 3); KO GBR (3, 3). **D** Content in 2-Cys Prxs (21 kDa band, see **F**). Values (arbitrary unit) are normalized with β-actin as internal control. **E** Ratio between hyperoxidized 2-Cys Prxs (Prx-$SO_{2/3}$H) and total 2-Cys Prxs at the 21 kDa band. WT PBS (3 males, 2 females); WT GBR (3, 2); KO PBS (3, 2); KO GBR (3, 2). For **B-E**: * $p<=0.05$, (*) $p=0.067$ (multiple comparisons using Tukey HSD test). Box plots depict medians and quartiles; bars show values in the 1.5 box length range. **F** Representative Western blot showing the band for β-actin and the bands at 21 and 24 kDa which are recognized by the antibodies against 2-Cys Prxs and against Prx-$SO_{2/3}$H. Note that the Prxs at 24 kDa was not different across groups and the Prx-$SO_{2/3}$H band at 24 kDa was hardly visible and therefore not analyzed.

Fig. 7. Long-term effects of early-life GBR treatment on oxidative stress, parvalbumin interneurons, perineuronal nets (PNNs), and microglia activation in the ACC of PD60 GRIN2A KO mice. A Number of parvalbumin-immunoreactive (PV-IR) cells. **B** Intensity (a.u.) of PV-IR within processes. **C** Intensity (a.u.) of labeling of WFA-PNNs. **D** Intensity (a.u.) of 8-oxo-dG-IR. **E** Number of Iba1-IR cells. **F** Number of CD68-IR cells. Different from KO: * $p<0.05$, ** $p<0.01$, *** $p<0.001$; different from WT: # $p<0.05$, # # $p<0.01$, # # # $p<0.001$ (multiple comparisons using Tukey HSD test or Games-Howell test) . For **A-D**: WT (2 males, 3 females);

KO (6, 2); KO GBR (4, 4). For **E-F**: WT (3 males, 2 females); KO (3, 2); KO GBR (3, 2). Box plots depict medians and quantiles; bars show values in the 1.5 box length range.

Fig. 8. Long-term effects of early-life GBR treatment on oxidative stress, parvalbumin interneurons, and perineuronal nets (PNNs) in the ACC of PD60 GRIN2A KO mice. Representative images of parvalbumin immunreactivity, WFA-labeled PNNs, and 8-oxo-dG labeling in the ACC of non-treated WT and KO mice, and GBR-treated KO mice. Scale: 50 μm.

Fig. 9. Long-term effects of early-life GBR treatment on microglia activation in the ACC of PD60 GRIN2A KO mice. Representative images of Iba1 and CD68 immunoreactivity in the ACC of non-treated WT and KO mice, and GBR-treated KO mice. Scale: 20 μm.

Fig. 10. Long-term effect of early-life GBR treatment on local high-frequency oscillatory activity induced in ACC slices of PD60 GRIN2A KO mice. Power spectrum (median) of neuronal activity induced in ACC slices by a mixture of carbachol, kainate, and quinpirole in (**A**) PBS- and GBR-treated WT mice and in (**B**) PBS- and GBR-treated KO mice. Power of β frequency (12-28 Hz) oscillations in (**C**) WT and (**D**) KO mice. Peak frequency of oscillations in (**E**) WT and (**F**) KO mice. Number of slices: 28 WT PBS, 25 WT GBR, 21 KO PBS, 34 KO GBR. Slices are from similar numbers of males and females. * $p<0.05$ (two-tailed Student t-test). Box plots depict medians and quartiles; bars show values in the 1.5 box length range.

References

Abekawa, T., Ito, K., Nakagawa, S., Koyama, T., 2007. Prenatal exposure to an NMDA receptor antagonist, MK-801 reduces density of parvalbumin-immunoreactive GABAergic neurons in the medial prefrontal cortex and enhances phencyclidine-induced hyperlocomotion but not behavioral sensitization to methamphetamine in postpubertal rats. Psychopharmacology 192:303-316.

Bartos, M., Vida, I., Jonas, P., 2007. Synaptic mechanisms of synchronized gamma oscillations in inhibitory interneuron networks. Nature Rev. Neurosci. 8:45-56.

Baxter, P.S., Bell, K.F., Hasel, P., Kaindl, A.M., Fricker, M., Thomson, D., Cregan, S.P., Gillingwater, T.H., Hardingham, G.E., 2015. Synaptic NMDA receptor activity is coupled to the transcriptional control of the glutathione system. Nature Comm. 6:6761.

Beasley, C.L., Reynolds, G.P., 1997. Parvalbumin-immunoreactive neurons are reduced in the prefrontal cortex of schizophrenics. Schizophr. Res. 24:349-355.

Behrens, M.M., Ali, S.S., Dao, D.N., Lucero, J., Shekhtman, G., Quick, K.L., Dugan, L.L., 2007. Ketamine-induced loss of phenotype of fast-spiking interneurons is mediated by NADPH-oxidase. Science 318:645-1647.

Beneyto, M., Meador-Woodruff, J.H., 2008. Lamina-specific abnormalities of NMDA receptor-associated postsynaptic protein transcripts in the prefrontal cortex in schizophrenia and bipolar disorder. Neuropsychopharmacology 33:2175-2186.

Berretta, S., Pantazopoulos, H., Markota, M., Brown, C., Batzianouli, E.T., 2015. Losing the sugar coating: potential impact of perineuronal net abnormalities on interneurons in schizophrenia. Schizophr. Res. 167:18-27.

Billingslea, E.N., Tatard-Leitman, V.M., Anguiano, J., Jutzeler, C.R., Suh, J., Saunders, J.A., Morita, S., Featherstone, R.E., Ortinski, P.I., Gandal, M.J., Lin, R., Liang, Y., Gur, R.E., Carlson, G.C., Hahn, C.G., Siegel, S.J., 2014. Parvalbumin cell ablation of NMDA-R1 causes increased resting network excitability with associated social and self-care deficits. Neuropsychopharmacology 39:1603-1613.

Bitanihirwe, B.K., Lim, M.P., Kelley, J.F., Kaneko, T., Woo, T.U., 2009. Glutamatergic deficits and parvalbumin-containing inhibitory neurons in the prefrontal cortex in schizophrenia. BMC Psychiatry 9: 71.

Burnashev, N., Szepetowski, P., 2015. NMDA receptor subunit mutations in neurodevelopmental disorders. Curr. Opin. Pharmacol. 20:73-82.

Cabungcal, J.H., Steullet, P., Kraftsik, R., Cuenod, M., Do, K.Q., 2013a. Early-life insults impair parvalbumin interneurons via oxidative stress: reversal by N-acetylcysteine. Biol. Psychiatry 73:574-582.

Cabungcal, J.H., Steullet, P., Morishita, H., Kraftsik, R., Cuenod, M., Hensch, T.K., Do, K.Q., 2013b. Perineuronal nets protect fast-spiking interneurons against oxidative stress. Proc. Natl. Acad. Sci. USA 110:9130-9135.

Cardin, J.A., Carlen, M., Meletis, K., Knoblich, U., Zhang, F., Deisseroth, K., Tsai, L.H., Moore, C.I., 2009. Driving fast-spiking cells induces gamma rhythm and controls sensory responses. Nature 459:663-667.

Carlen, M., Meletis, K., Siegle, J.H., Cardin, J.A., Futai, K., Vierling-Claassen, D., Ruhlmann, C., Jones, S.R., Deisseroth, K., Sheng, M., Moore, C.I., Tsai, L.H., 2012. A critical role for NMDA receptors in parvalbumin interneurons for gamma rhythm induction and behavior. Mol. Psychiatry 17:537-548.

Cho, K.K., Khibnik, L., Philpot, B.D., Bear, M.F., 2009. The ratio of NR2A/B NMDA receptor subunits determines the qualities of ocular dominance plasticity in visual cortex. Proc. Natl. Acad. Sci. USA 106:5377-5382.

Choi, Y., Chen, H.V., Lipton, S.A., 2001. Three pairs of cysteine residues mediate both redox and zn2+ modulation of the nmda receptor. J. Neurosci. 21:392-400.

Consortium, S.W.G.o.t.P.G., 2014. Biological insights from 108 schizophrenia-associated genetic loci. Nature 511:421-427.

Costa, R.O., Lacor, P.N., Ferreira, I.L., Resende, R., Auberson, Y.P., Klein, W.L., Oliveira, C.R., Rego, A.C., Pereira, C.M., 2012. Endoplasmic reticulum stress occurs downstream of GluN2B subunit of N-methyl-d-aspartate receptor in mature hippocampal cultures treated with amyloid-beta oligomers. Aging cell 11:823-833.

Coyle, J.T., Basu, A., Benneyworth, M., Balu, D., Konopaske, G., 2012. Glutamatergic synaptic dysregulation in schizophrenia: therapeutic implications. Handb. Exp. Pharmacol. 213:267-295.

Dityatev, A., Bruckner, G., Dityateva, G., Grosche, J., Kleene, R., Schachner, M., 2007. Activity-dependent formation and functions of chondroitin sulfate-rich extracellular matrix of perineuronal nets. Dev. Neurobiol. 67:570-588.

Do, K.Q., Cabungcal, J.H., Frank, A., Steullet, P., Cuenod, M., 2009. Redox dysregulation, neurodevelopment, and schizophrenia. Curr. Opin. Neurobiol. 19:220-230.

das Neves Duarte, J.M., Kulak, A., Gholam-Razaee, M.M., Cuenod, M., Gruetter, R., Do, K.Q., 2012. N-Acetylcysteine Normalizes Neurochemical Changes in the Glutathione-Deficient Schizophrenia Mouse Model During Development. Biol. Psychiatry 71:1006-14.

Dwir, D., Cabungcal, J.H., Steullet, P., Schnider, M., Cuénod, M., Do, K.Q., 2016. N-acetyl-cysteine and environmental enrichment reversed the long-lasting effect of oxidative stress on PVI circuitry: relevance for schizophrenia. Society for Neuroscience, Neuroscience planning 2016 (San Diego) abstract 269.10. http://www.sfn.org/annual-meeting/past-and-future-annual-meetings.

Enwright, J.F., Sanapala, S., Foglio, A., Berry, R., Fish, K.N., Lewis, D.A., 2016. Reduced Labeling of Parvalbumin Neurons and Perineuronal Nets in the Dorsolateral Prefrontal Cortex of Subjects with Schizophrenia. Neuropsychopharmacology 41:2206-2214.

Fagiolini, M., Katagiri, H., Miyamoto, H., Mori, H., Grant, S.G., Mishina, M., Hensch, T.K., 2003. Separable features of visual cortical plasticity revealed by N-methyl-D-aspartate receptor 2A signaling. Proc. Natl. Acad. Sci. USA 100:2854-2859.

Flatow, J., Buckley, P., Miller, B.J., 2013. Meta-analysis of oxidative stress in schizophrenia. Biol. Psychiatry 74:400-409.

Foscarin, S., Ponchione, D., Pajaj, E., Leto, K., Gawlak, M., Wilczynski, G.M., Rossi, F., Carulli, D., 2011. Experience-dependent plasticity and modulation of growth regulatory molecules at central synapses. PloS one 6(1):e16666.

Fuchs, E.C., Zivkovic, A.R., Cunningham, M.O., Middleton, S., Lebeau, F.E., Bannerman, D.M., Rozov, A., Whittington, M.A., Traub, R.D., Rawlins, J.N., Monyer, H., 2007. Recruitment of parvalbumin-positive interneurons determines hippocampal function and associated behavior. Neuron 53:591-604.

Gandal, M.J., Nesbitt, A.M., McCurdy, R.M., Alter, M.D., 2012. Measuring the maturity of the fast-spiking interneuron transcriptional program in autism, schizophrenia, and bipolar disorder. PloS one 7: e41215.

Ganguly, P., Holland, F.H., Brenhouse, H.C., 2015. Functional Uncoupling NMDAR NR2A Subunit from PSD-95 in the Prefrontal Cortex: Effects on Behavioral Dysfunction and Parvalbumin Loss after Early-Life Stress. Neuropsychopharmacology 40:2666-2675.

Hardingham, G.E., Do, K.Q., 2016. Linking early-life NMDAR hypofunction and oxidative stress in schizophrenia pathogenesis. Nature Rev. Neurosci. 17:125-134.

Hastings, T.G., Lewis, D.A., Zigmond, M.J., 1996. Role of oxidation in the neurotoxic effects of intrastriatal dopamine injections. Proc. Natl. Acad. Sci. USA 93:1956-1961.

Hirrlinger, J., Schulz, J.B., Dringen, R., 2002. Effects of dopamine on the glutathione metabolism of cultured astroglial cells: implications for Parkinson's disease. J. Neurochem. 82:458-467.

Homayoun, H., Moghaddam, B., 2007. NMDA receptor hypofunction produces opposite effects on prefrontal cortex interneurons and pyramidal neurons. J. Neurosci. 27:11496-11500.

Hu, H., Gan, J., Jonas, P., 2014. Interneurons. Fast-spiking, parvalbumin(+) GABAergic interneurons: from cellular design to microcircuit function. Science 345:1255263.

Jiang, Z., Rompala, G.R., Zhang, S., Cowell, R.M., Nakazawa, K., 2013. Social isolation exacerbates schizophrenia-like phenotypes via oxidative stress in cortical interneurons. Biol. Psychiatry 73:1024-1034.

Kim, S.Y., Cohen, B.M., Chen, X., Lukas, S.E., Shinn, A.K., Yuksel, A.C., Li, T., Du, F., Ongur, D., 2016. Redox Dysregulation in Schizophrenia Revealed by in vivo NAD+/NADH Measurement. Schizophr. Bull. 43:197-204.

, J.W., Davis, C.N., Tabarean, I., Conti, B., Bartfai, T., Behrens, M.M., 2006. A specific role for NR2A-containing NMDA receptors in the maintenance of parvalbumin and GAD67 immunoreactivity in cultured interneurons. J. Neurosci. 26:1604-1615.

Kocsis, B., Brown, R.E., McCarley, R.W., Hajos, M., 2013. Impact of ketamine on neuronal network dynamics: translational modeling of schizophrenia-relevant deficits. CNS Neurosci. Ther. 19:437-447.

Kohr, G., Eckardt, S., Luddens, H., Monyer, H., Seeburg, P.H., 1994. NMDA receptor channels: subunit-specific potentiation by reducing agents. Neuron 12:1031-1040.

Korotkova, T., Fuchs, E.C., Ponomarenko, A., von Engelhardt, J., Monyer, H., 2010. NMDA receptor ablation on parvalbumin-positive interneurons impairs hippocampal synchrony, spatial representations, and working memory. Neuron 68:557-569.

Lewis, D.A., Curley, A.A., Glausier, J.R., Volk, D.W., 2012. Cortical parvalbumin interneurons and cognitive dysfunction in schizophrenia. Trends Neurosci. 35:57-67.

Liu, R., Dang, W., Du, Y., Zhou, Q., Liu, Z., Jiao, K., 2015. Correlation of functional GRIN2A gene promoter polymorphisms with schizophrenia and serum D-serine levels. Gene 568:25-30.

Massi, L., Lagler, M., Hartwich, K., Borhegyi, Z., Somogyi, P., Klausberger, T., 2012. Temporal dynamics of parvalbumin-expressing axo-axonic and basket cells in the rat medial prefrontal cortex in vivo. J. Neurosci. 32:16496-16502.

Matta, J.A., Pelkey, K.A., Craig, M.T., Chittajallu, R., Jeffries, B.W., McBain, C.J., 2013. Developmental origin dictates interneuron AMPA and NMDA receptor subunit composition and plasticity. Nature Neurosci. 16:1032-1041.

Mauney, S.A., Athanas, K.M., Pantazopoulos, H., Shaskan, N., Passeri, E., Berretta, S., Woo, T.U., 2013. Developmental pattern of perineuronal nets in the human prefrontal cortex and their deficit in schizophrenia. Biol. Psychiatry 74:427-435.

McClure, E.A., Gipson, C.D., Malcolm, R.J., Kalivas, P.W., Gray, K.M., 2014. Potential role of N-acetylcysteine in the management of substance use disorders. CNS drugs 28:95-106.

McRae, P.A., Rocco, M.M., Kelly, G., Brumberg, J.C., Matthews, R.T., 2007. Sensory deprivation alters aggrecan and perineuronal net expression in the mouse barrel cortex. J. Neurosci. 27:5405-5413.

Pantazopoulos, H., Markota, M., Jaquet, F., Ghosh, D., Wallin, A., Santos, A., Caterson, B., Berretta, S., 2015. Aggrecan and chondroitin-6-sulfate abnormalities in schizophrenia and bipolar disorder: a postmortem study on the amygdala. Transl. Psychiatry 5:e496.

Paoletti, P., Bellone, C., Zhou, Q., 2013. NMDA receptor subunit diversity: impact on receptor properties, synaptic plasticity and disease. Nature Rev. Neurosci. 14:383-400.

Papadia, S., Soriano, F.X., Leveille, F., Martel, M.A., Dakin, K.A., Hansen, H.H., Kaindl, A., Sifringer, M., Fowler, J., Stefovska, V., McKenzie, G., Craigon, M., Corriveau, R., Ghazal, P., Horsburgh, K., Yankner, B.A., Wyllie, D.J., Ikonomidou, C., Hardingham, G.E., 2008. Synaptic NMDA receptor activity boosts intrinsic antioxidant defenses. Nature Neurosci. 11:476-487.

Poels, E.M., Kegeles, L.S., Kantrowitz, J.T., Javitt, D.C., Lieberman, J.A., Abi-Dargham, A., Girgis, R.R., 2014. Imaging glutamate in schizophrenia: review of findings and implications for drug discovery. Mol. Psychiatry 19:20-29.

Powell, S.B., Sejnowski, T.J., Behrens, M.M., 2012. Behavioral and neurochemical consequences of cortical oxidative stress on parvalbumin-interneuron maturation in rodent models of schizophrenia. Neuropharmacology 62:1322-1331.

Rojo, A.I., McBean, G., Cindric, M., Egea, J., Lopez, M.G., Rada, P., Zarkovic, N., Cuadrado, A., 2014. Redox control of microglial function: molecular mechanisms and functional significance. Antioxid. Redox Signal. 21:1766-1801.

Sakimura, K., Kutsuwada, T., Ito, I., Manabe, T., Takayama, C., Kushiya, E., Yagi, T., Aizawa, S., Inoue, Y., Sugiyama, H., et al., 1995. Reduced hippocampal LTP and spatial learning in mice lacking NMDA receptor epsilon 1 subunit. Nature 373:151-155.

Schiavone, S., Jaquet, V., Sorce, S., Dubois-Dauphin, M., Hultqvist, M., Backdahl, L., Holmdahl, R., Colaianna, M., Cuomo, V., Trabace, L., Krause, K.H., 2012. NADPH oxidase elevations in pyramidal neurons drive psychosocial stress-induced neuropathology. Transl. Psychiatry 2:e111.

Slaker, M., Barnes, J., Sorg, B.A., Grimm, J.W., 2016. Impact of Environmental Enrichment on Perineuronal Nets in the Prefrontal Cortex following Early and Late Abstinence from Sucrose Self-Administration in Rats. PloS one 11(12): e0168256.

Sohal, V.S., Zhang, F., Yizhar, O., Deisseroth, K., 2009. Parvalbumin neurons and gamma rhythms enhance cortical circuit performance. Nature 459:698-702.

Steiner, J., Walter, M., Glanz, W., Sarnyai, Z., Bernstein, H.G., Vielhaber, S., Kastner, A., Skalej, M., Jordan, W., Schiltz, K., Klingbeil, C., Wandinger, K.P., Bogerts, B., Stoecker, W., 2013. Increased prevalence of diverse N-methyl-D-aspartate glutamate receptor antibodies in patients with an initial diagnosis of schizophrenia: specific relevance of IgG NR1a antibodies for distinction from N-methyl-D-aspartate glutamate receptor encephalitis. JAMA Psychiatry 70:271-278.

Steullet, P., Cabungcal, J.H., Coyle, J., Didriksen, M., Gill, K., Grace, A.A., Hensch, T.K., LaMantia, A.S., Lindemann, L., Maynard, T.M., Meyer, U., Morishita, H., O'Donnell, P., Puhl, M., Cuenod, M., Do, K.Q., 2017. Oxidative stress-driven parvalbumin interneuron impairment as a common mechanism in models of schizophrenia. Mol. Psychiatry 22:936-943.

Steullet, P., Cabungcal, J.H., Cuenod, M., Do, K.Q., 2014. Fast oscillatory activity in the anterior cingulate cortex: dopaminergic modulation and effect of perineuronal net loss. Front. Cellular Neurosci. 8:244.

Steullet, P., Cabungcal, J.H., Monin, A., Dwir, D., O'Donnell, P., Cuenod, M., Do, K.Q., 2016. Redox dysregulation, neuroinflammation, and NMDA receptor hypofunction: A "central hub" in schizophrenia pathophysiology? Schizophr. Res. 176:41-51.

Tarabeux, J., Kebir, O., Gauthier, J., Hamdan, F.F., Xiong, L., Piton, A., Spiegelman, D., Henrion, E., Millet, B., Fathalli, F., Joober, R., Rapoport, J.L., DeLisi, L.E., Fombonne, E., Mottron, L., Forget-Dubois, N., Boivin, M., Michaud, J.L., Drapeau, P., Lafreniere, R.G., Rouleau, G.A., Krebs, M.O., 2011. Rare mutations in N-methyl-D-aspartate glutamate receptors in autism spectrum disorders and schizophrenia. Transl. Psychiatry 1:e55.

Turnock-Jones, J.J., Jennings, C.A., Robbins, M.J., Cluderay, J.E., Cilia, J., Reid, J.L., Taylor, A., Jones, D.N., Emson, P.C., Southam, E., 2009. Increased expression of the NR2A NMDA receptor subunit in the prefrontal cortex of rats reared in isolation. Synapse 63:836-846.

Wang, C.Z., Yang, S.F., Xia, Y., Johnson, K.M., 2008. Postnatal phencyclidine administration selectively reduces adult cortical parvalbumin-containing interneurons. Neuropsychopharmacology 33:2442-2455.

Wang, D., Fawcett, J., 2012. The perineuronal net and the control of CNS plasticity. Cell Tissue Res. 349:147-160.

Yao, J.K., Keshavan, M.S., 2011. Antioxidants, redox signaling, and pathophysiology in schizophrenia: an integrative view. Antioxid. Redox Signal. 15:2011-2035.

Zhang, Z., Sun, Q.Q., 2011. Development of NMDA NR2 subunits and their roles in critical period maturation of neocortical GABAergic interneurons. Dev. Neurobiology 71:221-245.

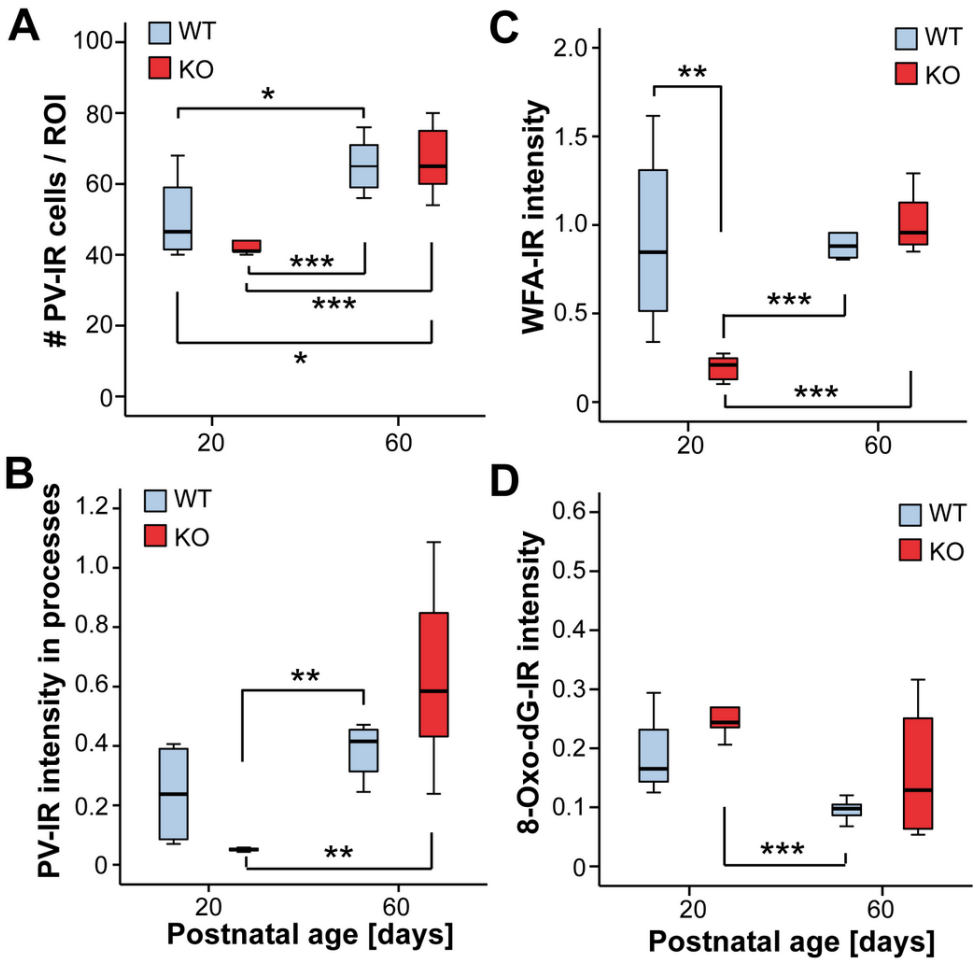
A
PV-IR cells / ROI
WT
KO
B
PV-IR intensity in processes
Postnatal age [days]
C
WFA-IR intensity
D
8-Oxo-dG-IR intensity
Postnatal age [days]

Figure 1

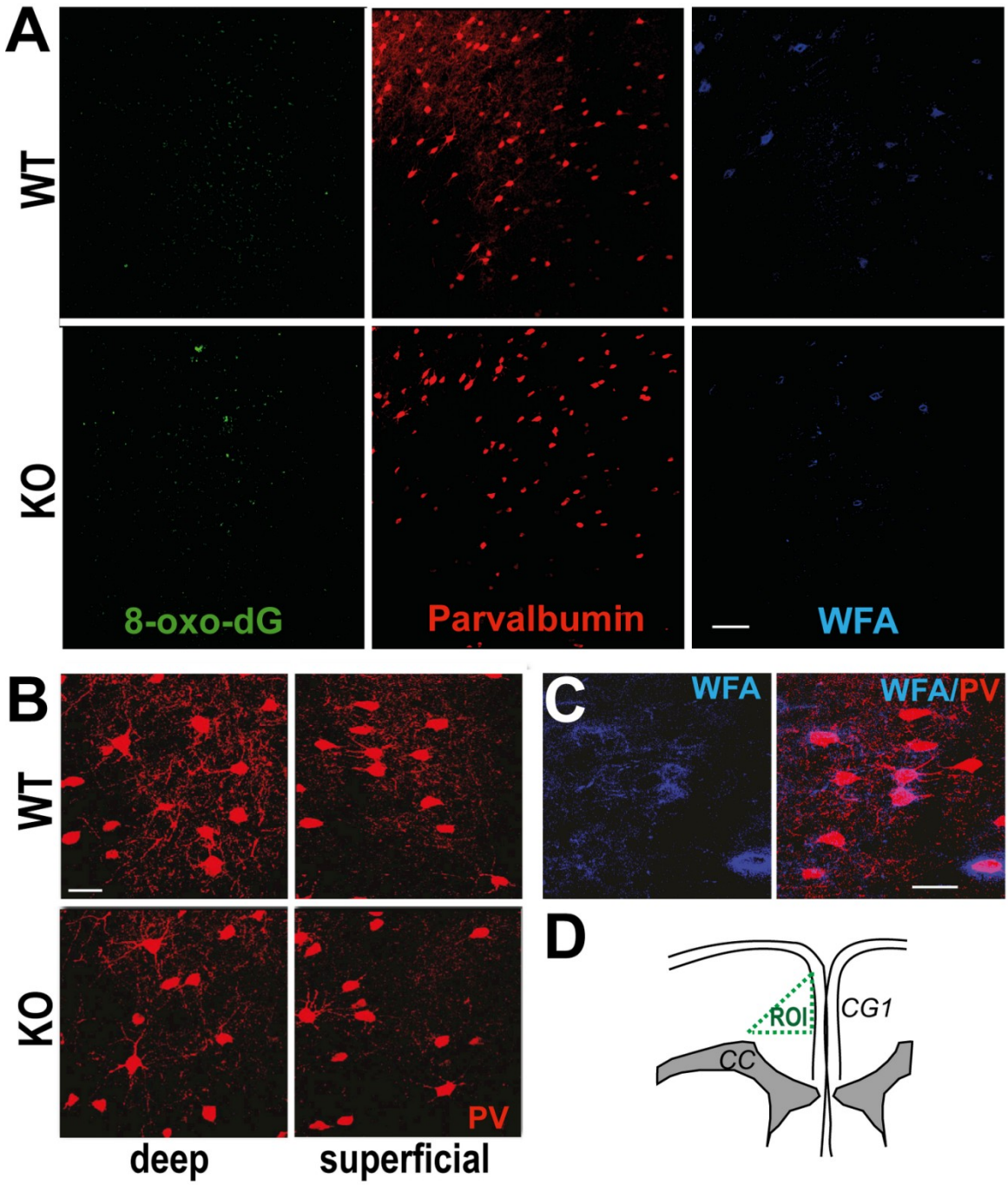
A
WT
KO
8-oxo-dG
Parvalbumin
WFA
B
WT
KO
deep
superficial
PV
C
WFA
WFA/PV
D
ROI
CG1
CC

Figure 2.

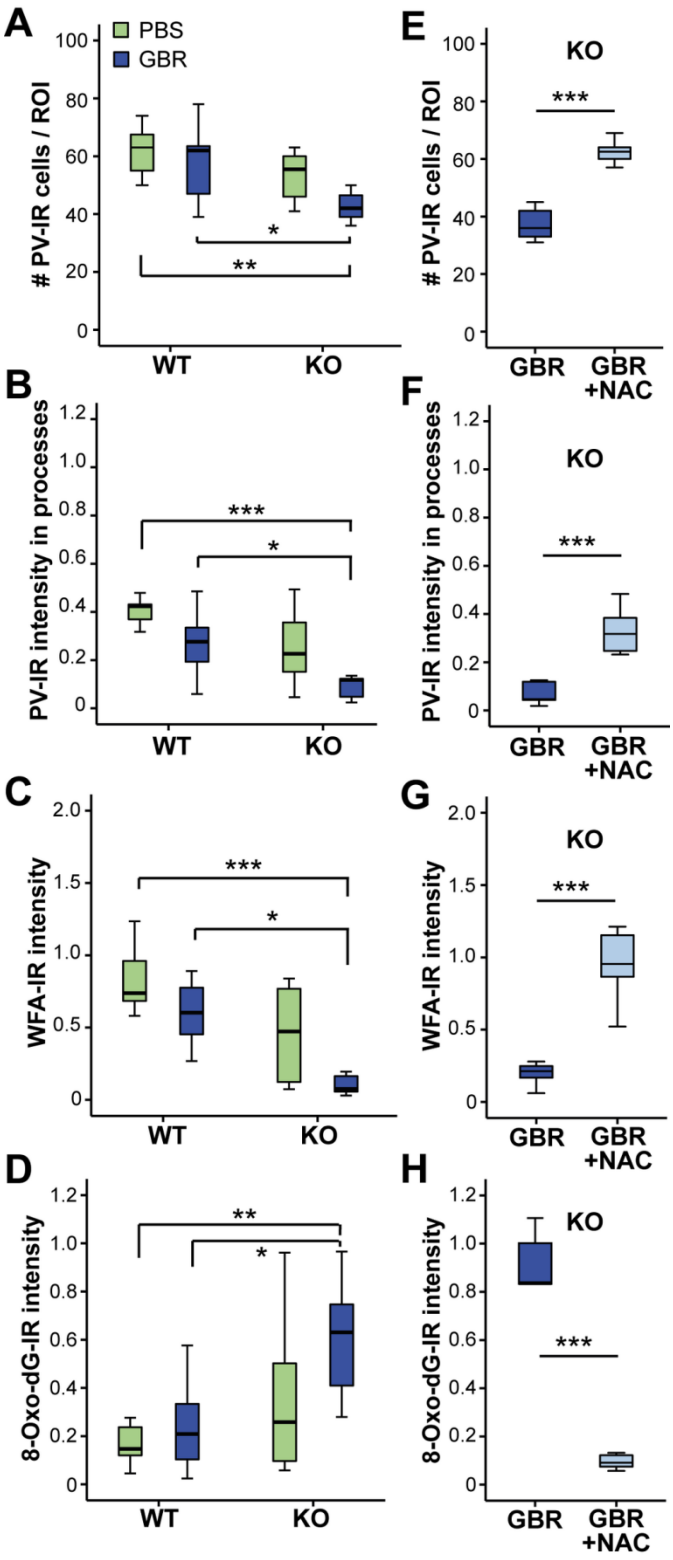
A
PBS
GBR
PV-IR cells / ROI
WT
KO
B
PV-IR intensity in processes
C
WFA-IR intensity
D
8-Oxo-dG-IR intensity
E
KO
GBR
GBR +NAC
F
G
H

Figure 3.

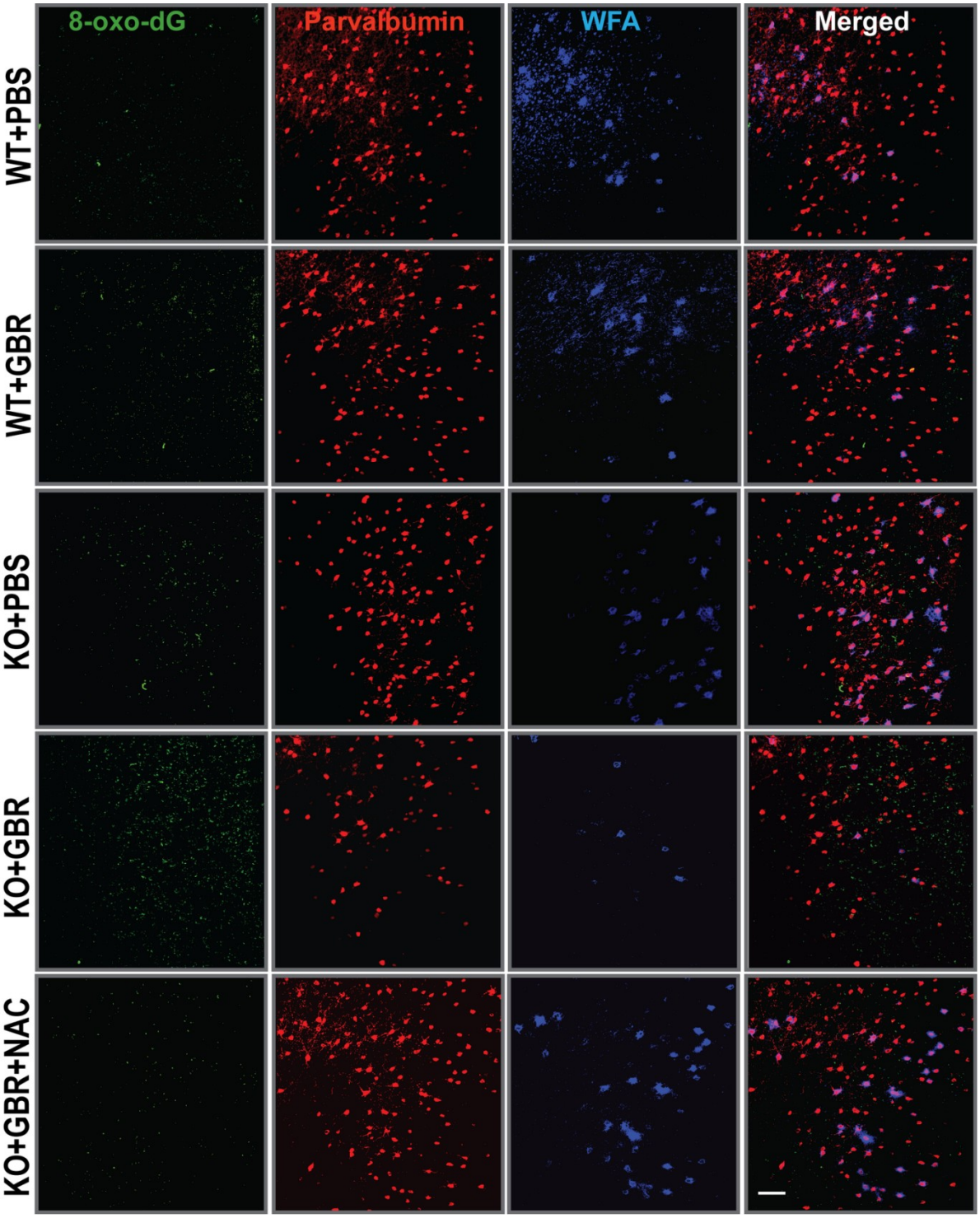
8-oxo-dG
Parvalbumin
WFA
Merged
WT+PBS
WT+GBR
KO+PBS
KO+GBR
KO+GBR+NAC

Figure 4.

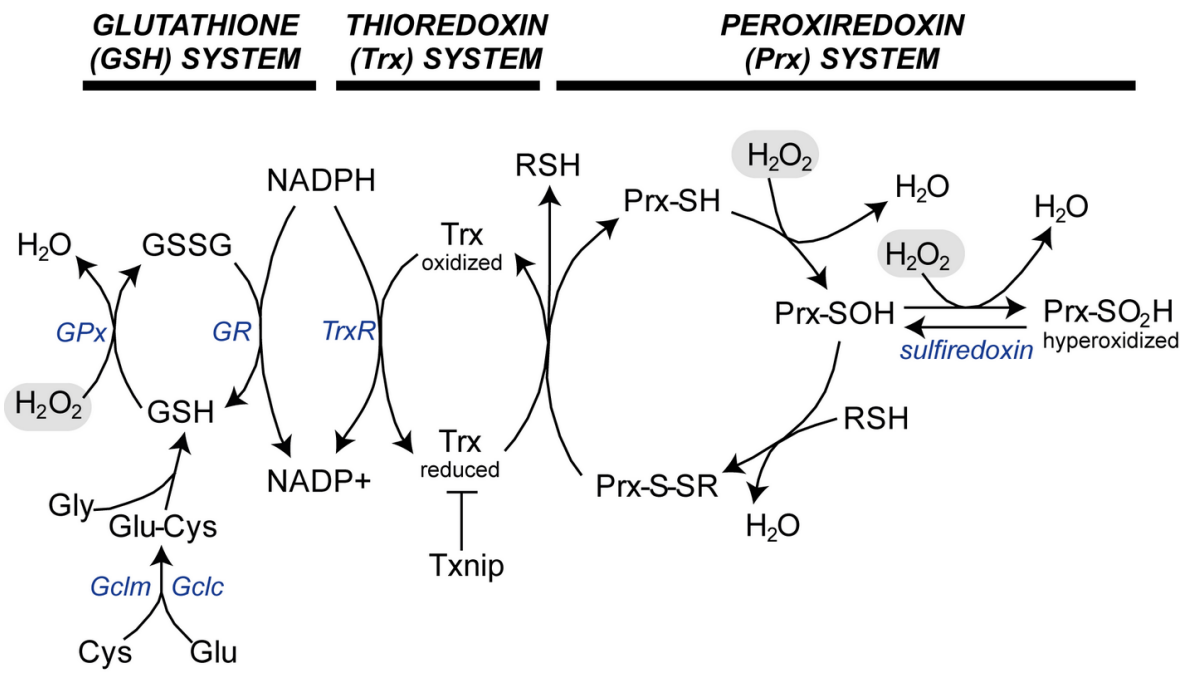
GLUTATHIONE (GSH) SYSTEM
THIOREDOXIN (Trx) SYSTEM
PEROXIREDOXIN (Prx) SYSTEM
NADPH
RSH
H_2O_2
Prx-SH
H_2O
H_2O
H_2O
GSSG
Trx oxidized
H_2O_2
GPx
GR
TrxR
Prx-SOH
$Prx-SO_2H$ hyperoxidized
sulfiredoxin
H_2O_2
GSH
RSH
Trx reduced
NADP+
Prx-S-SR
Gly
Glu-Cys
H_2O
Txnip
Gclm
Gclc
Cys
Glu

Figure 5.

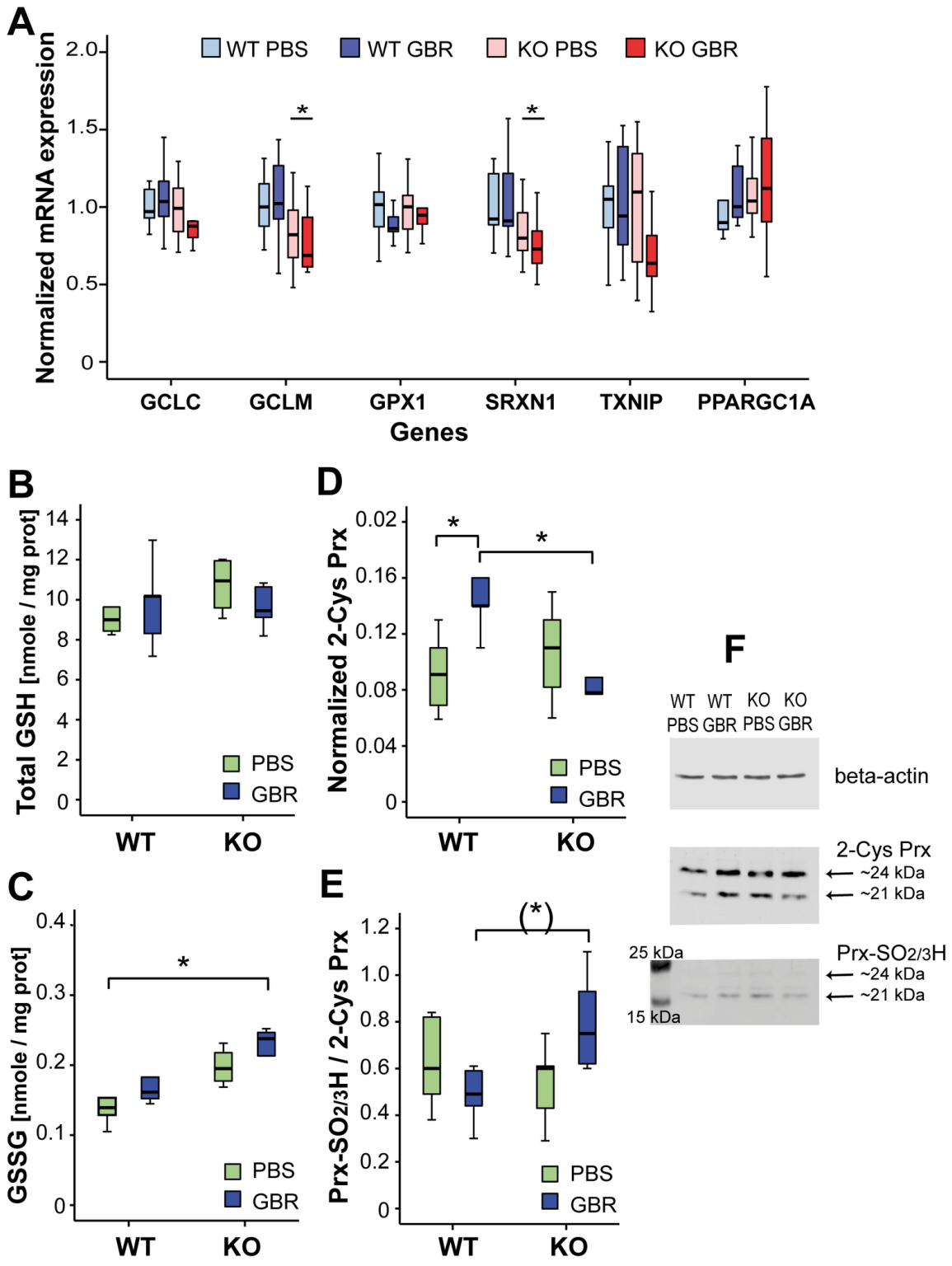
A
WT PBS
WT GBR
KO PBS
KO GBR
Normalized mRNA expression
2.0
1.5
1.0
0.5
0
*
*
GCLC
GCLM
GPX1
SRXN1
TXNIP
PPARGC1A
Genes
B
Total GSH [nmole / mg prot]
14
12
10
8
6
4
2
0
PBS
GBR
WT
KO
D
Normalized 2-Cys Prx
0.02
0.16
0.12
0.08
0.04
0
*
*
PBS
GBR
WT
KO
F
WT WT KO KO
PBS GBR PBS GBR
beta-actin
2-Cys Prx
~24 kDa
~21 kDa
25 kDa
15 kDa
Prx-SO2/3H
~24 kDa
~21 kDa
C
GSSG [nmole / mg prot]
0.4
0.3
0.2
0.1
0
*
PBS
GBR
WT
KO
E
Prx-SO2/3H / 2-Cys Prx
1.2
1.0
0.8
0.6
0.4
0.2
0
(*)
PBS
GBR
WT
KO

Figure 6.

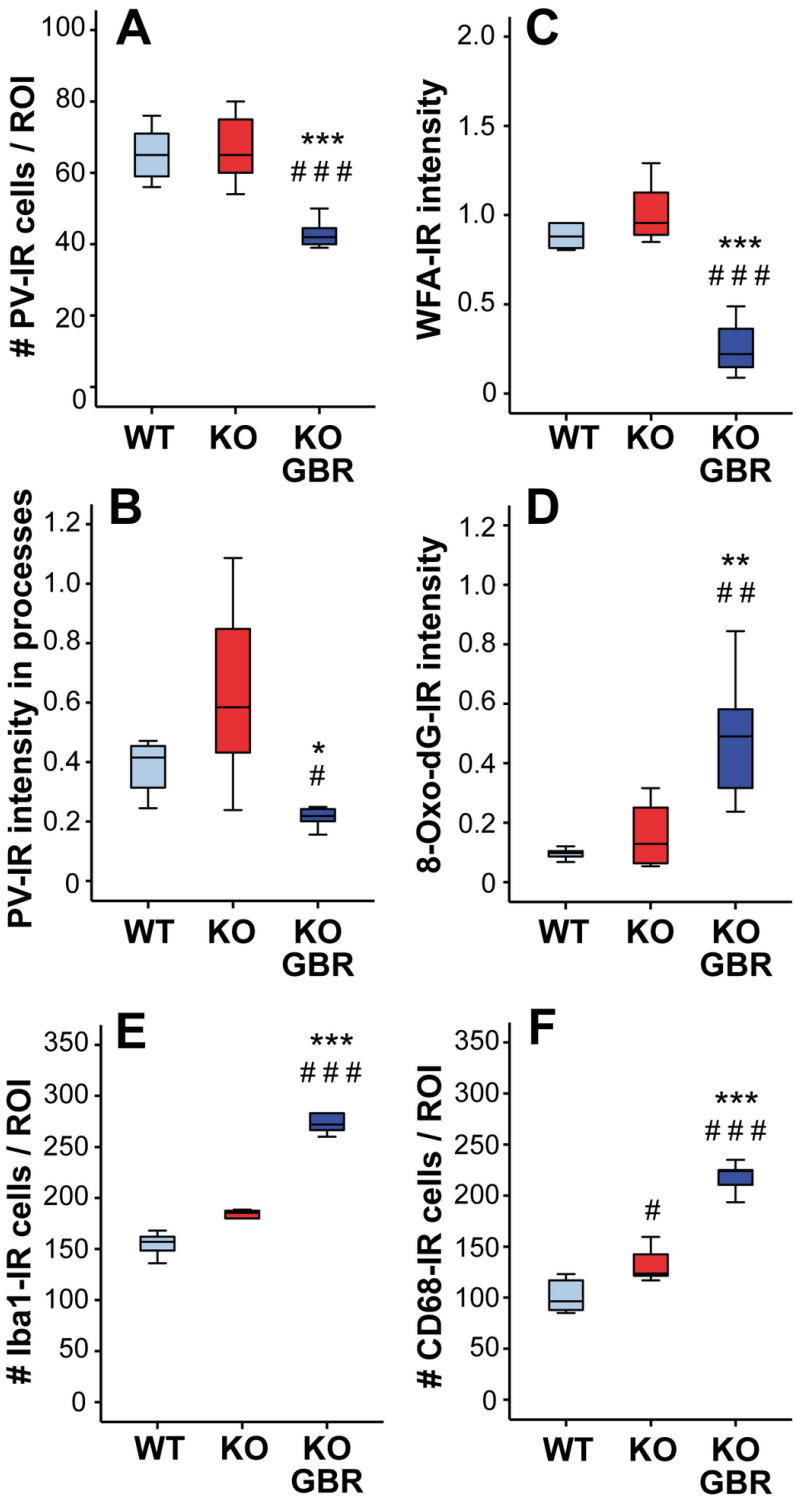
A
PV-IR cells / ROI
100
80
60
40
20
0
***
###
WT
KO
KO GBR
C
WFA-IR intensity
2.0
1.5
1.0
0.5
0
***
###
WT
KO
KO GBR
B
PV-IR intensity in processes
1.2
1.0
0.8
0.6
0.4
0.2
0
*
#
WT
KO
KO GBR
D
8-Oxo-dG-IR intensity
1.2
1.0
0.8
0.6
0.4
0.2
0
**
##
WT
KO
KO GBR
E
Iba1-IR cells / ROI
350
300
250
200
150
100
50
0
***
###
WT
KO
KO GBR
F
CD68-IR cells / ROI
350
300
250
200
150
100
50
0
***
###
#
WT
KO
KO GBR

Figure 7.

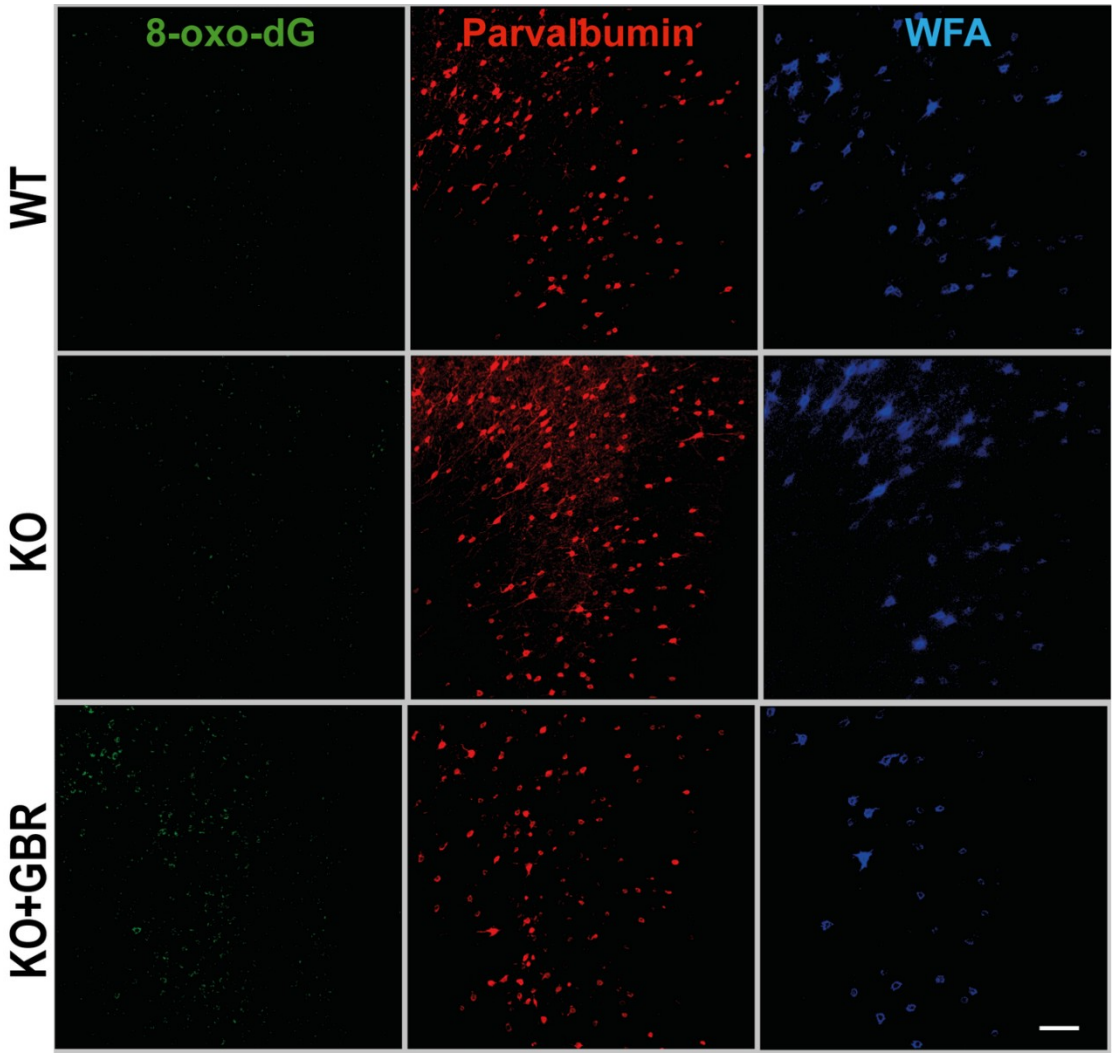

Figure 8.

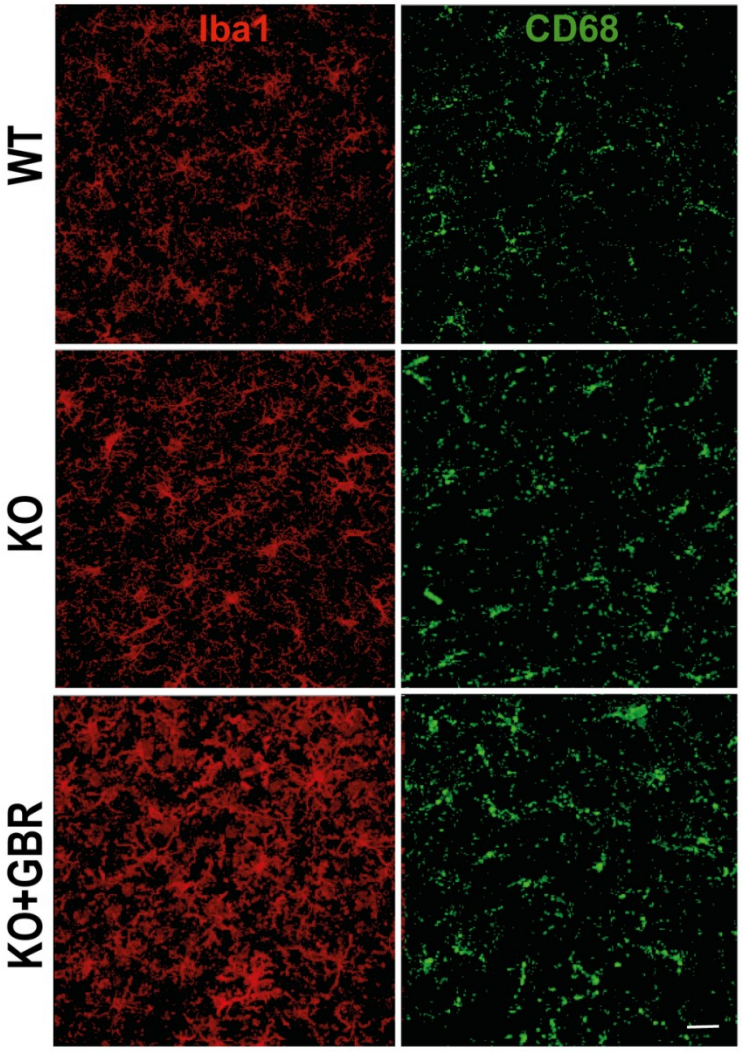

Figure 9.

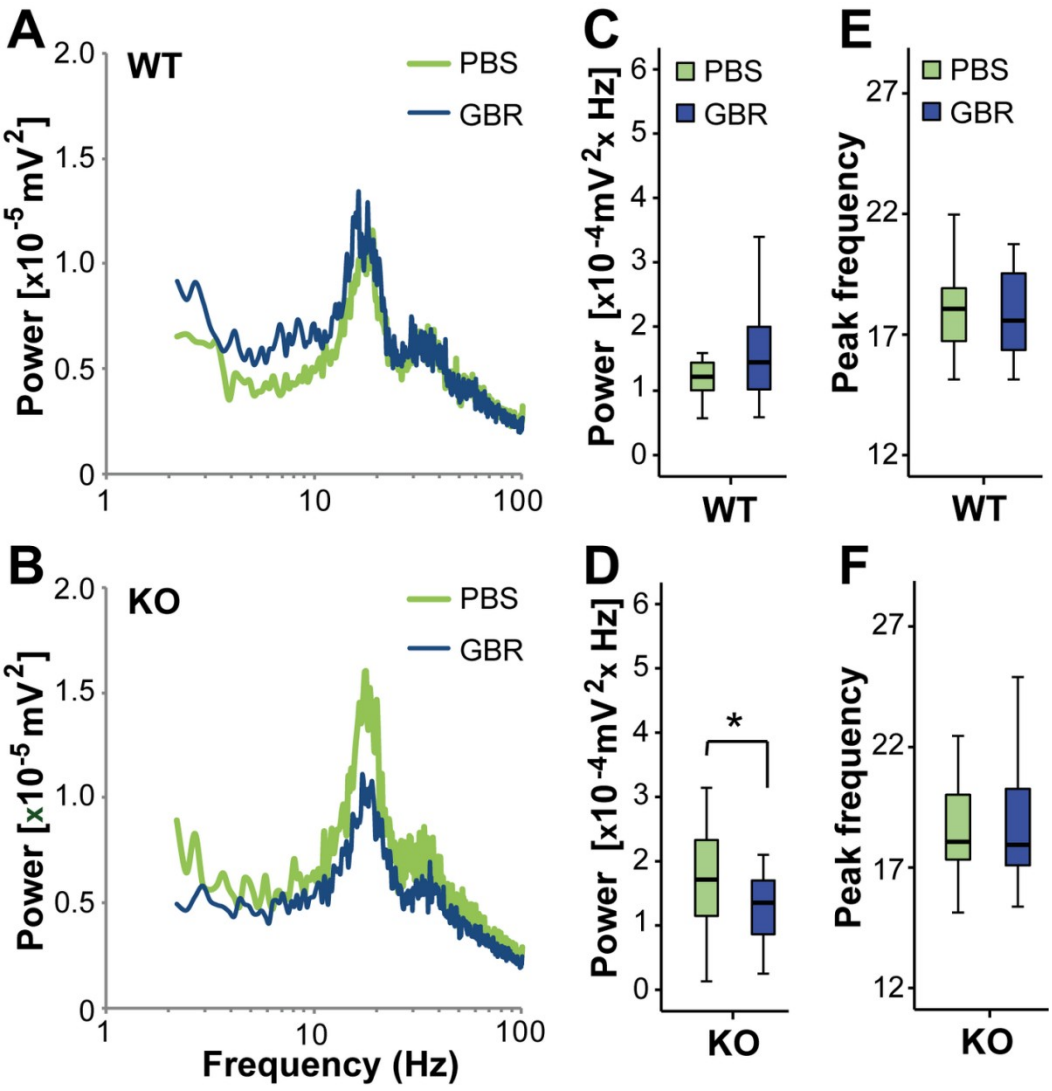
A
WT
PBS
GBR
Power [x10-5 mV2]
2.0
1.5
1.0
0.5
0
1
10
100
B
KO
PBS
GBR
Power [x10-5 mV2]
Frequency (Hz)
C
PBS
GBR
Power [x10-4mV2x Hz]
WT
D
Power [x10-4mV2x Hz]
*
KO
E
PBS
GBR
Peak frequency
27
22
17
12
WT
F
Peak frequency
KO

Figure 10.